



Structure of cell networks critically determines oscillation regularity

Hiroshi Kori ^{a,b,*}, Yoji Kawamura ^c, Naoki Masuda ^{b,d,**}

^a Division of Advanced Sciences, Ochanomizu Academic Production, Ochanomizu University, Tokyo 112-8610, Japan

^b PRESTO, Japan Science and Technology Agency, Kawaguchi 332-0012, Japan

^c Institute for Research on Earth Evolution, Japan Agency for Marine-Earth Science and Technology, Yokohama 236-0001, Japan

^d Department of Mathematical Informatics, The University of Tokyo, Tokyo 113-8656, Japan

ARTICLE INFO

Article history:

Received 7 September 2011

Received in revised form

21 November 2011

Accepted 7 December 2011

Available online 16 December 2011

Keywords:

Synchronization

Network

Noise

Circadian rhythm

Heart

ABSTRACT

Biological rhythms are generated by pacemaker organs, such as the heart pacemaker organ (the sinoatrial node) and the master clock of the circadian rhythms (the suprachiasmatic nucleus), which are composed of a network of autonomously oscillatory cells. Such biological rhythms have notable periodicity despite the internal and external noise present in each cell. Previous experimental studies indicate that the regularity of oscillatory dynamics is enhanced when noisy oscillators interact and become synchronized. This effect, called the collective enhancement of temporal precision, has been studied theoretically using particular assumptions. In this study, we propose a general theoretical framework that enables us to understand the dependence of temporal precision on network parameters including size, connectivity, and coupling intensity; this effect has been poorly understood to date. Our framework is based on a phase oscillator model that is applicable to general oscillator networks with any coupling mechanism if coupling and noise are sufficiently weak. In particular, we can manage general directed and weighted networks. We quantify the precision of the activity of a single cell and the mean activity of an arbitrary subset of cells. We find that, in general undirected networks, the standard deviation of cycle-to-cycle periods scales with the system size N as $1/\sqrt{N}$, but only up to a certain system size N^* that depends on network parameters. Enhancement of temporal precision is ineffective when $N > N^*$. We provide an example in which temporal precision considerably improves with increasing N while the level of synchrony remains almost constant; temporal precision and synchrony are independent dynamical properties. We also reveal the advantage of long-range interactions among cells to temporal precision.

© 2011 Elsevier Ltd. All rights reserved.

1. Introduction

Biological rhythms such as heartbeats and sleep-waking cycles are essential in living organisms. Many biological rhythms are generated by pacemaker organs composed of autonomously rhythmic cells. For example, the heart pacemaker (*i.e.*, the sinoatrial node) is the source of electric waves propagating from within the heart, which cause the contraction of cardiac cells (Glass, 2001). The suprachiasmatic nucleus (SCN), which is a network of clock cells located in the brain, orchestrates the circadian (*i.e.*, approximately 24 h) activity of the entire body. Each clock cell has a circadian rhythm in its electric activity owing to the gene regulatory network within the cell, and a population of clock cells synchronizes its activity through neural interactions (Reppert and Weaver, 2002). The medullary pacemaker nucleus in

electric fish is the pacemaker for the electric discharges emitted by electric fish, which are used for object detection and communication with other electric fish (Heiligenberg *et al.*, 1981).

Cell dynamics involve fluctuations resulting from various types of internal and external noise. However, oscillations in pacemaker organs such as the sinoatrial node in the heart, the SCN, and the medullary pacemaker nucleus in electric fish are highly precise. For example, the daily onset of activity in certain mammals and birds has a standard deviation (SD) of a few minutes even in the absence of environmental information (Enright, 1980). In addition, the electric organ discharge pattern in certain electric fish has a standard deviation of as little as 0.02% of the average period (Moortgat *et al.*, 2000b).

Experiments by Clay and DeHaan (1979) provided an important clue for understanding the mechanisms underlying precise oscillations. They prepared clusters of cultivated cardiac cells, ranging in size from 1 to ~ 100 , and observed the beatings of individual cells. They found that the SD of inter-beat intervals decreases with the number of component cells in the cluster (N) roughly as $SD \propto 1/\sqrt{N}$. Therefore, precision in individual cell oscillations is enhanced as the number of cells increases. Note that this scaling, which is reminiscent of the

* Corresponding author at: Division of Advanced Sciences, Ochanomizu Academic Production, Ochanomizu University, Tokyo 112-8610, Japan. Tel.: +81 3 5978 5067.

** Corresponding author at: Department of Mathematical Informatics, The University of Tokyo, Tokyo 113-8656, Japan. Tel.: +81 3 5841 6931.

E-mail addresses: kori.hiroshi@ocha.ac.jp (H. Kori), masuda@mist.i.u-tokyo.ac.jp (N. Masuda).

central limit theorem, is not at all trivial. This is because oscillators are synchronized and thus strongly correlated, while the central limit theorem is applicable to an ensemble of independent elements.

The decrease in SD as N increases, the so-called collective enhancement of temporal precision, has attracted considerable attention (Enright, 1980; Winfree, 2001; Clay and DeHaan, 1979; Moortgat et al., 2000a,b; Herzog et al., 2004; Kojima et al., 2006; Sherman et al., 1988; Garcia-Ojalvo et al., 2004; Vasalou et al., 2009; Rappel and Karma, 1996; Needleman et al., 2001; Ly and Ermentrout, 2010; Tabareau et al., 2010). There is a large body of experimental (Clay and DeHaan, 1979; Moortgat et al., 2000b; Herzog et al., 2004; Kojima et al., 2006), numerical (Sherman et al., 1988; Moortgat et al., 2000a; Garcia-Ojalvo et al., 2004; Vasalou et al., 2009), and analytical (Rappel and Karma, 1996; Needleman et al., 2001; Ly and Ermentrout, 2010; Tabareau et al., 2010) studies. Theoretically, it has been shown that the average activity of all oscillators on the all-to-all network (*i.e.*, the complete graph) obeys $SD \propto 1/\sqrt{N}$ (Rappel and Karma, 1996; Needleman et al., 2001). However, most analytical studies are based on rather strong assumptions about coupling topology (*e.g.*, all-to-all) or coupling mechanism (*e.g.*, gap-junction type). Moreover, little is known about temporal precision in single cell activity or ensemble activity for a subset of cells in an entire network. Note that in the experiments by Clay and DeHaan (1979), the behavior $SD \propto 1/\sqrt{N}$ was found for single cells and not for the entire network.

In this paper, we theoretically study the effect of cell-to-cell communication on temporal precision. By using a phase oscillator model and assuming full synchrony (*i.e.*, all oscillators are synchronized in frequency) and weak noise, we analytically derive the dependence of temporal precision on various network parameters, including size, connectivity, and coupling intensity. Our framework allows us to handle directed and weighted networks as well as temporal precision in the activity of arbitrary subsets of cells. Note that temporal precision is related to but different from the stability of synchronization, which has been extensively studied (Pecora and Carroll, 1998; Arenas et al., 2008). Temporal precision is much less understood than the stability of synchronization.

We treated a similar issue in our previous paper (Masuda et al., 2010), where we analyzed long-time phase diffusion in coupled oscillators. We show that temporal precision, which is based on cycle-to-cycle periods, is associated with short-time phase diffusion. Therefore, we here extend our previous analysis to the case of an arbitrary time scale. This extension turns out to be crucial for the understanding of the collective enhancement of temporal precision particularly in the case of large system sizes or small coupling strengths.

We begin by describing the numerical results for two biological pacemaker models: network of the FitzHugh–Nagumo oscillators and that of circadian oscillators. These models have distinct oscillation and coupling mechanisms. For different networks including all-to-all coupling, lattices with nearest-neighbor coupling, and the random graph, we observe that there is a common dependence of temporal precision on network size N . The SD of cycle-to-cycle periods decreases as $1/\sqrt{N}$ in small networks, but approaches an asymptotic value as N increases. That is, there is a crossover. Then, we develop a theory for obtaining an explicit expression for the SD of the cycle-to-cycle period. In particular, we find the condition for the behavior $SD \propto 1/\sqrt{N}$ and the dependence of the crossover point N^* on network parameters. We also demonstrate the advantage of long-range interactions among cells to temporal precision. Finally, we discuss the implications of our theory.

2. Numerical results

First, we present the numerical results for two mathematical models describing biological oscillations (see Appendix A for the details of the models). We used FHN oscillators with gap-junction coupling as a model of oscillatory cardiac or neural cells. We also employed a previously proposed model for the SCN (*i.e.*, a population of circadian clock cells) (Locke et al., 2008), which is referred to as the SCN model.

2.1. Regularization of oscillation

Fig. 1(a,c,e) and (b,d,f) presents the waveforms obtained from the FHN and SCN models of different network sizes, respectively. The average cycle-to-cycle periods are depicted by dotted lines in each panel to illuminate the variations in cycle-to-cycle periods. The properties of each constituent cell were kept constant, while the connectivity between the cells is different. Typical waveforms of uncoupled cells ($N=2$) are shown in Fig. 1(a,b). When the cells are coupled sufficiently strongly, the system synchronizes stably (Fig. 1(c,d)). Fig. 1(c,d) indicates that waveforms in the presence of coupling are regularized as compared to the waveforms of isolated cells [Fig. 1(a,b)]. In particular, the variation in the cycle-to-cycle period decreases. When 100 oscillators are coupled [Fig. 1(e,f)], the variation appears to be even smaller. When cells are coupled, individual cell oscillations are not only synchronized but also regularized, and the oscillation appears to be more regular for a larger system size.

2.2. Limit to the enhancement of temporal precision

To quantify the dependence of temporal precision on network parameters, we measured the coefficient of variation (CV), which is the SD of the cycle-to-cycle period divided by the mean period. A cycle-to-cycle period is defined by an interval Δt between two successive passages of an observed variable (x_i) across a specified threshold value x_{th} (Fig. 2). We set $x_{th} = 0.4$ and 2.0 for the FHN and SCN models, respectively. We discard $\Delta t < T_{min}$, where T_{min} is sufficiently smaller than a typical oscillation period, to exclude noise-driven rapid threshold crossing. Specifically, we set $T_{min} = 50$ and 15 in the FHN and SCN models, respectively. We confirmed that our numerical results are insensitive to the choice of T_{min} values. The CV is defined as

$$CV = \frac{SD}{\tau}, \quad (1)$$

where τ and SD are the mean and the SD of a series of Δt , respectively.

Here we investigate the FHN model on networks of different types and different sizes. We assume that the system is composed of identical cells subjected to weak noise. Fig. 3(a) shows the CV of individual cell oscillations in the FHN model on the all-to-all network of size N . The results for different coupling strength values, κ , are plotted using different symbols. We find that

- (i) CV is proportional to $1/\sqrt{N}$ for small N values for each κ .
- (ii) CV approaches a constant value for large N values for each κ ; *i.e.*, there is a crossover.
- (iii) the crossover point N^* increases with κ .

We observe similar behavior for the square lattice and the random graph, as shown in Fig. 3(b) and (c), respectively.

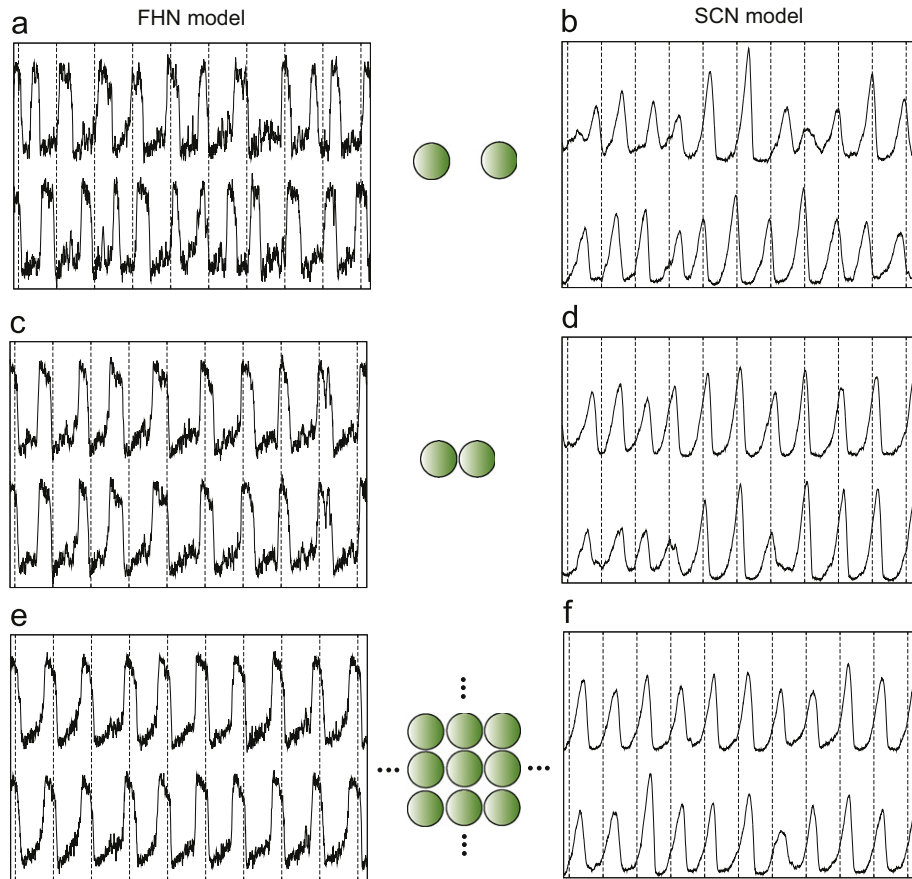


Fig. 1. Waveforms obtained from biological oscillator models. We present the time series of $x_i(t)$ of (a,b) two isolated cells ($\kappa = 0, N = 2$), (c,d) two coupled cells ($\kappa > 0, N = 2$), and (e,f) two cells in 100 coupled cells ($\kappa > 0, N = 100$) in (a,c,e) the FHN model and (b,d,f) the SCN model. In (e), we employ the one-dimensional lattice with an open boundary condition and show the waveforms of two neighboring cells. In (f), we employ the all-to-all network ($A_{ij} = 1/N$ for $1 \leq i, j \leq N$). We set $\rho = 0.1$ in all panels and (a,b) $\kappa = 0$, (c,e) $\kappa = 2$, and (d,f) $\kappa = 1$.

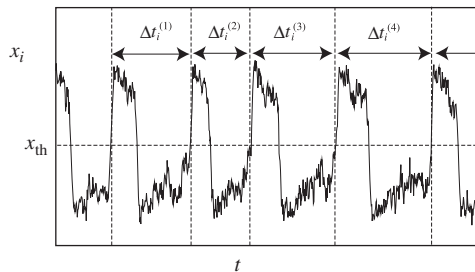


Fig. 2. Schematic illustration of the concept of cycle-to-cycle period.

2.3. Relationship between temporal precision and synchronization level

A natural question is whether the enhanced synchronization induces the collective enhancement of temporal precision. To examine this possibility, we measured the distance δ between the actual state and the in-phase state (see Appendix A for the definition of δ) for the all-to-all network. As shown in Fig. 3(d), the level of synchrony is independent of N for each κ value. We also confirmed that, in the FHN model on a square lattice, δ even increases with N although the CV decreases (results not shown). Thus, the enhancement of temporal precision by an increase in N is not attributed to the improvement in synchronization.

2.4. Temporal precision for the ensemble activity

In nature, rhythmic output from a pacemaker organ is usually generated by an ensemble of multiple cells. For example,

rhythmic electroactivity propagating within the heart is thought to originate from cells on the surface of the sinoatrial node. The SCN consists of various neural populations, and each population forms a particular pattern of efferent projections to other parts of the brain (Abrahamson and Moore, 2001). This anatomical fact suggests that the SCN's output is generated by a combination of a subset of neurons rather than by the uniform average of the entire organ.

Therefore, we investigated the CV of the ensemble activity of a subset of cells on the all-to-all network. The ensemble activity is defined by the average waveform of M ($1 \leq M \leq N$) cells:

$$X(t) = \frac{1}{M} \sum_{i=1}^M x_i(t), \quad (2)$$

where the measured ensemble is assumed to consist of oscillators x_1, \dots, x_M . The cycle-to-cycle period and the CV for the ensemble activity are defined similar to the case of single cell activity (Fig. 2). In Fig. 4, we present the CV measured for the average waveform with different values of M in the FHN model on the all-to-all network. For M smaller than N , properties (i)–(iii) listed above are preserved. In addition, we find that

- (iv) the crossover point N^* increases with ensemble size M ,
- (v) for $M=N$, the CV is proportional to $1/\sqrt{N}$ for any N ; i.e., there is no crossover.

We also confirmed that the same properties hold true for the FHN model on two-dimensional lattices and for the SCN model on the all-to-all network and the two-dimensional lattice.

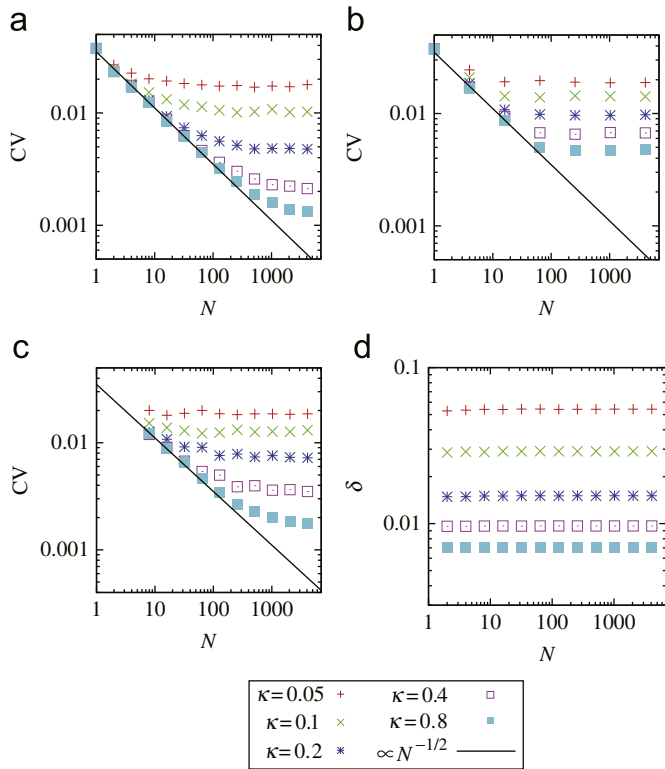


Fig. 3. CV for single cell oscillations and synchronization distance δ in the FHN model. (a,b,c) CV values for single cell oscillations on (a) the all-to-all network, (b) the square lattice, and (c) the undirected random graph of size N . (d) Distance δ from in-phase synchrony in the all-to-all network. In (a) and (d), we set $A_{ij} = 1/N$ for $1 \leq i, j \leq N$. In (b), the CV of the oscillator at the center of the square lattice with an open boundary condition is presented. We set $A_{ij} = 1/4$ with cell j adjacent to cell i and $A_{ij} = 0$ otherwise. In (c), the CV value at given κ and N values is defined as $\langle CV_i \rangle \equiv \sum_{i=1}^N CV_i/N$ for a single realization of the network. We set $A_{ij} = A_{ji} = 1/8$ with probability $p = 8/N$ ($1 \leq i < j \leq N$), and $A_{ij} = 0$ otherwise. The lines are guides to the eyes. We considered identical cells and weak noise ($\rho = 0.01$). The average period τ is almost constant ($\tau \approx 177$) irrespective of N and κ .

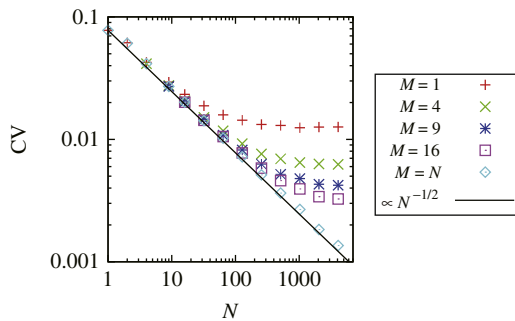


Fig. 4. CV for ensemble activity of M cells in the FHN model on the all-to-all network. Parameter values are the same as in Fig. 3, except $\rho = 0.0256$ and $K = 0.2$. The line is a guide to the eyes.

2.5. Case of strong noise and heterogeneity

So far, we have assumed an ideal case: identical oscillators and weak noise. To simulate more realistic situations, we now consider networks composed of heterogeneous cells subjected to relatively strong noise. As examples, we measure the CV for the FHN model on the square lattice and for the SCN model on the all-to-all network (Fig. 5). In the FHN model, we made one of the parameter values heterogeneous in order to obtain the

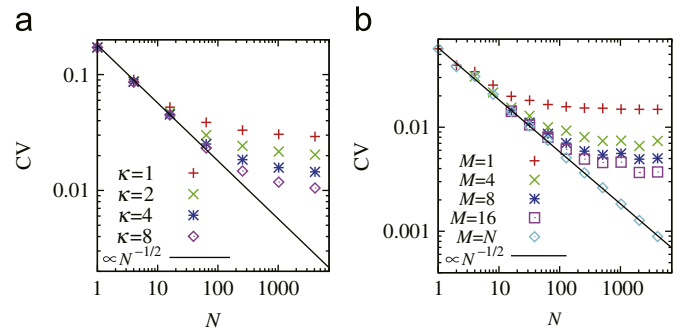


Fig. 5. CV for biological models composed of heterogeneous cells subjected to relatively strong noise. (a) CV for single cell oscillations in the FHN model on the square lattice. We set $\rho = 0.09$. (b) CV for the ensemble activity of M cells in the SCN model on the all-to-all network. We set $\rho = 0.04$ and $K = 12$. The all-to-all network and the square lattice are the same as those in Fig. 3(a) and (b), respectively. The lines are guides to the eyes.

distribution of natural periods of cells as $\tau_i \approx 133 \pm 3$ (mean \pm SD). In the SCN model, the time scales of the cells were made heterogeneous such that $\tau_i \approx 23.4 \pm 1.2$. The latter situation is consistent with the experimental observation by Honma et al. (1998). In all cases, we apply sufficiently strong coupling to ensure that the oscillators are well synchronized. Under this condition, as seen in Fig. 5, all properties (i)–(v) hold true.

3. Theory

We found, numerically that properties (i)–(v) hold true in various situations. In the following, we develop a theory for relating temporal precision to network parameters by assuming weak coupling and weak noise. Under this assumption, a large class of oscillator systems including the models considered above are reduced to the phase model (see Appendix B and Winfree, 1967; Kuramoto, 1984) given by

$$\dot{\phi}_i(t) = \omega_i + \kappa \sum_{j=1}^N A_{ij} f(\phi_j - \phi_i) + \sqrt{D} \xi_i(t), \quad (3)$$

where ϕ_i and ω_i ($1 \leq i \leq N$) are the phase and intrinsic frequency of the i th oscillator, respectively; $A = (A_{ij})$ is the weighted adjacency matrix with its element A_{ij} equal to the intensity of the coupling from the j th to i th oscillators; κ is the overall coupling intensity; $f(\cdot)$ is a 2π -periodic function; $\xi_i(t)$ is independent white Gaussian noise with $E[\xi_i(t)] = 0$ and $E[\xi_i(t)\xi_j(t')] = \delta_{ij}\delta(t-t')$, where E represents the expectation; and D is the strength of the noise. The adjacency matrix A is allowed to be asymmetric, weighted, and to possess negative components. Extension of the following results in the case of ij -dependent coupling function $f_{ij}(\cdot)$ and i -dependent noise strength D_i is straightforward. For clarity of the presentation, we focus on Eq. (3). We assume that all the oscillators are synchronized in frequency; i.e., all the oscillators have the actual frequency Ω owing to the effect of coupling. Synchronization usually occurs when coupling is sufficiently strong compared to noise and heterogeneity in ω_i .

One oscillation cycle corresponds to an increase in the phase by 2π . More precisely, the k th cycle-to-cycle period of the i th oscillator is defined by $\Delta t_i^{(k)} = t_i^{(k)} - t_i^{(k-1)}$, where $t_i^{(k)}$ is the first passage time for $\phi_i(t)$ to exceed $2k\pi$ (Fig. 6). Because we assumed that all the oscillators are synchronized to Ω , the expected value of $\Delta t_i^{(k)}$ (τ) is independent of i and is given as

$$\tau \equiv E[\Delta t_i^{(k)}] = \frac{2\pi}{\Omega}, \quad (4)$$

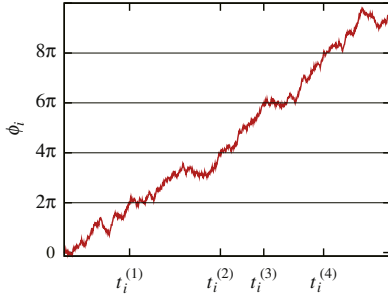


Fig. 6. First passage time for a phase oscillator.

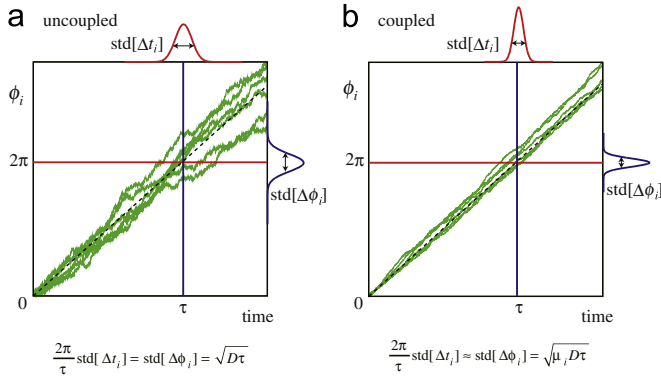


Fig. 7. Schematic illustration of our approximation to the cycle-to-cycle variation. Green trajectories represent different realizations of the phase $\phi_i(t)$ of a single oscillator in (a) uncoupled and (b) coupled cases, where we set $\phi_i(0) = 0$. The red curves on the top of each panel represent distribution function $P_t(t)$ obtained from the first passage time of $\phi_i(t) = 2\pi$ in different realizations. Our concern is its standard deviation, $SD_i = \text{std}[\Delta t_i]$. The blue curves on the right of each panel represent distribution function $P_\phi(\phi_i)$ obtained from different realizations of $\phi_i(\tau)$, where τ is the mean period, and its standard deviation is denoted by $\text{std}[\Delta\phi_i]$. We approximate $\text{std}[\Delta t_i]$ using $\text{std}[\Delta\phi_i]$. Suppose that $P_t(t)dt = P_\phi(\phi_i)d\phi_i$. On average, the phase crosses 2π with slope $2\pi/\tau$, i.e., $d\phi_i/dt = 2\pi/\tau$. We thus obtain Eq. (7). For uncoupled oscillators ($\kappa = 0$), our model corresponds to the Wiener process with a constant drift. In this case, Eq. (7) is exact, and we obtain $(2\pi/\tau)\text{std}[\Delta t_i] = \text{std}[\Delta\phi_i] = \sqrt{D\tau}$ (Gerstner and Kistler, 2002). We also know that Eq. (7) is asymptotically exact in the one-dimensional Ornstein–Uhlenbeck process for weak noise (Gerstner and Kistler, 2002). For coupled oscillators ($\kappa > 0$), however, our model (3) is a multivariate Ornstein–Uhlenbeck process when linearized. Even in this case, as is numerically confirmed in the examples shown in Figs. 8–11, Eq. (7) provides a suitable approximation.

where the statistical averages are taken over different k values. The temporal precision of the i th oscillator is characterized by

$$SD_i \equiv \text{std}[\Delta t_i] = \sqrt{\text{var}[\Delta t_i]} = \sqrt{E[(\Delta t_i^{(k)} - \tau)^2]}. \quad (5)$$

The CV for the i th oscillator is equal to

$$CV_i \equiv \frac{SD_i}{\tau}. \quad (6)$$

To obtain the dependence of SD_i on network parameters, we employ an approximation given by

$$\frac{2\pi}{\tau} \text{std}[\Delta t_i] \approx \text{std}[\Delta\phi_i], \quad (7)$$

where $\Delta\phi_i \equiv \phi_i(t+\tau) - \phi_i(t) - 2\pi$ (Fig. 7). For an isolated oscillator obeying $\dot{\phi}_i = \omega_i + \sqrt{D}\zeta_i(t)$, one immediately finds that $\text{var}[\Delta\phi_i] = D\tau$, where $\tau_i = 2\pi/\omega_i$. When oscillators are coupled and synchronized with frequency Ω , we write

$$\text{var}[\Delta\phi_i] = \mu_i D\tau. \quad (8)$$

We refer to μ_i as the noise scaling factor of the i th oscillator (Fig. 7). By combining Eqs. (5), (7) and (8), we have

$$SD_i \approx \frac{\sqrt{D\tau^3\mu_i}}{2\pi}. \quad (9)$$

To obtain an expression for μ_i , we assume that noise is sufficiently weak and linearize Eq. (3) around the synchronized state. The synchronized solution $\phi_i^s(t)$ ($1 \leq i \leq N$) is represented as

$$\phi_i^s(t) = \Omega t + \psi_i, \quad (10)$$

where Ω and ψ_i are the constants derived by setting $\dot{\phi}_i = \Omega$ and $D=0$ in Eq. (3); i.e.,

$$\Omega = \omega_i + \kappa \sum_{j=1}^N A_{ij} f(\psi_j - \psi_i). \quad (11)$$

By introducing a small deviation

$$\theta_i(t) = \phi_i(t) - \phi_i^s(t), \quad (12)$$

we obtain

$$\dot{\theta}_i(t) = \kappa \sum_{j=1}^N w_{ij}(\theta_j - \theta_i) + \sqrt{D}\zeta_i(t), \quad (13)$$

where $w_{ij} = A_{ij} f'(\psi_j - \psi_i)$ is the effective coupling weight. For convenience, we rewrite Eq. (13) as

$$\dot{\theta}_i(t) = -\kappa \sum_{j=1}^N L_{ij}\theta_j + \sqrt{D}\zeta_i(t), \quad (14)$$

where $L = (L_{ij})$ is the Jacobian matrix with its element L_{ij} given by

$$L_{ij} = \begin{cases} -w_{ij} & \text{for } i \neq j, \\ \sum_{i' \neq i} w_{i'i} & \text{for } i = j. \end{cases} \quad (15)$$

Note that L has a zero eigenvalue with the corresponding right eigenvector

$$\mathbf{u}^{(1)} = \frac{1}{\sqrt{N}}(1, \dots, 1)^T. \quad (16)$$

Furthermore, because of the assumption of the stability of the synchronized state, the real parts of the other $N-1$ eigenvalues of L are positive, i.e., $0 \equiv \lambda_1 < \text{Re } \lambda_2 \leq \dots \leq \text{Re } \lambda_N$. The assumption of the stability holds true when $w_{ij} \geq 0$ ($1 \leq i, j \leq N$) and the network described by the adjacency matrix (w_{ij}) is strongly connected (Ermentrout, 1992; Agaev and Chebotarev, 2000; Arenas et al., 2008). For more general cases, the stability condition is nontrivial.

For in-phase synchrony (i.e., $\psi_i = 0$ for $1 \leq i \leq N$ in Eq. (10)), which occurs when the heterogeneity in the network and in individual oscillators is sufficiently small and/or the coupling is sufficiently strong, we obtain $w_{ij} \propto A_{ij}$ for $1 \leq i, j \leq N$. In this case, L is the network Laplacian generalized for a directed and weighted network (Newman, 2010), given by

$$L_{ij} \begin{cases} -A_{ij} & \text{for } i \neq j, \\ \sum_{i' \neq i} A_{i'i} & \text{for } i = j. \end{cases} \quad (17)$$

Note that L is symmetric when the adjacency matrix A is symmetric.

As shown in Appendix C, for any diagonalizable matrix L , we obtain $\mu_i = C_{ii}$, where

$$C_{ij} \equiv \frac{E[(\theta_i(t+\tau) - \theta_i(t))(\theta_j(t+\tau) - \theta_j(t))]}{D\tau} \\ = \frac{V_{11}}{N} + \sum_{m, n(m+n > 2)}^N \frac{2 - e^{-\kappa\lambda_m\tau} - e^{-\kappa\lambda_n\tau}}{\kappa(\lambda_m + \lambda_n)\tau} V_{mn} u_i^{(m)} u_j^{(n)}. \quad (18)$$

Here $\mathbf{u}^{(n)} = (u_i^{(n)})$ and $\mathbf{v}^{(n)}$ are, respectively, the right and left eigenvectors of L that satisfy the orthogonality and normalization

conditions; i.e., $\mathbf{L}\mathbf{u}^{(n)} = \lambda_n \mathbf{u}^{(n)}$, $\mathbf{v}^{(n)}L = \lambda_n \mathbf{v}^{(n)}$, and $\mathbf{v}^{(m)}\mathbf{u}^{(n)} = \delta_{mn}$; and $V_{mn} = \mathbf{v}^{(m)} \cdot \mathbf{v}^{(n)}$.

For symmetric L , which is the case for in-phase synchrony on undirected networks, Eq. (18) becomes much simpler. Because all the eigenvalues are real, $\mathbf{u}^{(n)} = \mathbf{v}^{(n)\top}$, $V_{mn} = \mathbf{u}^{(m)} \cdot \mathbf{u}^{(n)} = \delta_{mn}$ for $1 \leq m, n \leq N$, and $\sum_{i=1}^N \mathbf{u}_i^{(1)} \propto \mathbf{u}^{(1)}$, $\mathbf{u}^{(n)} = \mathbf{0}$ for $n \geq 2$, we obtain

$$\mu_i = \frac{1}{N} + \sum_{n=2}^N \frac{1 - e^{-\kappa \lambda_n \tau}}{\kappa \lambda_n \tau} u_i^{(n)} u_i^{(n)}. \quad (19)$$

Moreover, because of the normalization condition, $\sum_{i=1}^N u_i^{(n)} u_i^{(n)} = 1$, the mean of μ_i over the entire network, $\langle \mu \rangle = \sum_{i=1}^N \mu_i / N$, is independent of the eigenvectors and is given by

$$\langle \mu \rangle = \frac{1}{N} + \frac{1}{N} \sum_{n=2}^N \frac{1 - e^{-\kappa \lambda_n \tau}}{\kappa \lambda_n \tau}. \quad (20)$$

Note that the first term on the right-hand side of Eqs. (19) and (20) is associated with the eigenvector corresponding to a homogeneous phase shift given by Eq. (16), which is the perturbation along the synchronized state. The second term on the right-hand side of Eqs. (19) and (20) is associated with the eigenvectors transverse to the synchronized state.

3.1. Dependence of the crossover point N^* on coupling strength κ

Henceforth, we assume that τ is independent of κ and N . We also assume that L is symmetric in this subsection. If the eigenvalue spectrum converges to a certain density function $q(\lambda)$ as $N \rightarrow \infty$, the second term on the right-hand side of Eq. (20) also converges:

$$\frac{1}{N} \sum_{n=2}^N \frac{1 - e^{-\kappa \lambda_n \tau}}{\kappa \lambda_n \tau} \rightarrow \mu_\infty \equiv \int_0^\infty q(\lambda) \frac{1 - e^{-\kappa \lambda \tau}}{\kappa \lambda \tau} d\lambda \quad (N \rightarrow \infty). \quad (21)$$

In Section 3.4, we will demonstrate that the convergence occurs in the all-to-all and ring networks. Spectra of finite dimensional lattices (Mohar, 1991), uncorrelated random graphs with arbitrary degree distributions (Samukhin et al., 2008), and the small-world network with a fixed expected degree (Monasson, 1999) also converge. In such networks, the N -dependence of the second term on the right-hand side of Eq. (20) is not strong. We thus approximate

$$\langle \mu \rangle \approx \frac{1}{N} + \mu_\infty. \quad (22)$$

By equating the first and second terms in Eq. (22), we estimate the crossover point as $N^* \approx 1/\mu_\infty$. For $N \ll N^*$, the first term dominates, so that the SD, which is proportional to $\sqrt{\mu_i}$ (see Eq. (9)), decreases proportionally to $1/\sqrt{N}$. For $N \gg N^*$, the SD is approximately constant.

Since μ_∞ monotonically decreases with increasing κ , N_* increases with κ . Furthermore, if the second smallest eigenvalue λ_2 is nonvanishing in the limit $N \rightarrow \infty$ (which is the case, for example, in the all-to-all network and various random networks including small-world networks Monasson, 1999; Samukhin et al., 2008) and κ is so large that $e^{-\kappa \lambda_2 \tau} \ll 1$, we can neglect $e^{-\kappa \lambda_n \tau}$ in the numerator of μ_∞ in Eq. (21) to obtain $\mu_\infty \propto 1/\kappa$. Then, the crossover point scales as

$$N^* \propto \kappa. \quad (23)$$

3.2. Dependence of the crossover point N^* on ensemble size M

By assuming in-phase synchrony, we calculate the scaling factor of the noise reduction for the ensemble activity of an arbitrary set of oscillators. We rearrange the oscillator indices and

write the ensemble activity as

$$X(t) = \sum_{i=1}^M \zeta_i x_i(t), \quad (24)$$

where $\zeta_i \geq 0$ is an arbitrary constant with the normalization condition $\sum_{i=1}^M \zeta_i = 1$. When the deviation θ_i from in-phase synchrony (i.e., $\psi_i = 0$ for $1 \leq i \leq N$ in Eq. (10)) is small for each oscillator, the phase of $X(t)$ is approximated by

$$\Phi(t) = \sum_{i=1}^M \zeta_i \phi_i(t) = \Omega t + \sum_{i=1}^M \zeta_i \theta_i(t). \quad (25)$$

Then, similar to the case of individual cell oscillations, we define the scaling factor μ_ϕ for the ensemble activity as

$$\text{var}[\Delta\Phi] = \mu_\phi D\tau, \quad (26)$$

where $\Delta\Phi = \Phi(t+\tau) - \Phi(t) - 2\pi$. We then obtain

$$\begin{aligned} \mu_\phi &= \frac{\text{var}[\Delta\Phi]}{D\tau} = \sum_{i,j=1}^M \zeta_i \zeta_j \frac{\text{E}[(\theta_i(t+\tau) - \theta_i(t))(\theta_j(t+\tau) - \theta_j(t))]}{D\tau} \\ &= \sum_{i,j=1}^M \zeta_i \zeta_j C_{ij}. \end{aligned} \quad (27)$$

Henceforth, we assume $\zeta_i = 1/M$ for $1 \leq i \leq M$, as is the case in Figs. 4 and 5(b).

There are notable properties for symmetric L (see Appendix D). When $M=N$ (i.e., $X(t)$ is the mean activity of the entire network), we obtain

$$\mu_\phi = \frac{1}{N}, \quad (28)$$

that is, there is no crossover. For $M < N$, μ_ϕ generally depends on the choice of M oscillators. However, if we randomly choose M oscillators out of N oscillators, where $1 \ll M \ll N$, we estimate

$$\mu_\phi \approx \frac{1}{N} + \frac{1}{MN} \sum_{n=2}^N \frac{1 - e^{-\kappa \lambda_n \tau}}{\kappa \lambda_n \tau} \approx \frac{1}{N} + \frac{\mu_\infty}{M}. \quad (29)$$

In this case, the lower bound of the SD is inversely proportional to \sqrt{M} and the crossover point increases as

$$N^* \propto M. \quad (30)$$

As shown later, this estimation is asymptotically exact for the all-to-all network.

3.3. Remarks on directed networks

The behavior $\text{CV} \propto 1/\sqrt{N}$ is obtained for $N < N^*$ when the Jacobian L is symmetric, which is the case when a network is undirected and the oscillators are synchronized in phase. We refer to this situation as “democratic” because symmetric L implies that the action and reaction between any two nodes are balanced.

For asymmetric L , Eq. (18) implies that the SD at small N values decreases as $\sqrt{V_{11}/N}$ instead of $1/\sqrt{N}$. In Masuda et al. (2010), we analyzed the long-time diffusion property of Eq. (3) to obtain $\sigma^2 \equiv \lim_{\Delta t \rightarrow \infty} \text{var}[(\theta_i(t+\Delta t) - \theta_i(t))/(D\Delta t)] = V_{11}/N$ through a different technique. This previous result is consistent with that obtained in the present paper because σ^2 corresponds to phase diffusion after infinitely many cycles, and the second term on the right-hand side of Eq. (18) vanishes with this limit. Furthermore, we showed in Masuda et al. (2010) that $\sqrt{V_{11}/N}$ is larger than or equal to $1/\sqrt{N}$ for asymmetric L . For example, in directed scale-free networks, which is a strongly heterogeneous network, we obtained $\sqrt{V_{11}/N} \propto N^{-\beta}$ with $0 \leq \beta \leq 1/2$; the effect of collective enhancement is significantly weaker. Moreover, the scaling $\sqrt{V_{11}/N} = N^{-1/2}$ can be violated even when a network is

undirected. This is the case when the synchronized state is not in-phase but accompanies a wave pattern. Wave patterns arise when the network is spatially extended (such as Euclidean lattices) and the natural frequency is sufficiently heterogeneous (Kuramoto, 1984; Blasius and Tönjes, 2005). In this case, V_{11}/N decreases with N for small N values but approaches a constant value for large N values. Thus, strongly asymmetric connectivity and/or strong heterogeneity in the oscillator's properties can hamper the collective enhancement of temporal precision.

3.4. Examples and numerical verification

To demonstrate and numerically confirm our analytical results, we investigate the phase model (Eq. (3)) on several networks. In numerical simulations, we set $\omega_i = 1$, $f(\phi) = \sin \phi$, and $\sqrt{D} = 0.01$ in Eq. (3). In the example networks, all the oscillators synchronize in phase in the absence of noise. Thus, $w_{ij} = A_{ij}$ and $\Omega = \omega$ for any coupling strength κ and any N . Note that the dependence of the CV on κ and N is only through the SD because $\tau = 2\pi/\omega$ is constant. In the following, we show the values of the normalized CV that is actual CV values divided by the CV of isolated oscillators, shown as $\sqrt{D}\tau/2\pi$. Our theory predicts that $CV_i \approx \sqrt{\mu_i}$ and $CV_\Phi \approx \sqrt{\mu_\Phi}$.

Two asymmetrically coupled elements: The first example is two asymmetrically coupled elements ($N=2$): $w_{12} = p$ and $w_{21} = 1-p$ (Fig. 8). In this case, we have $\lambda_1 = 0, \lambda_2 = -1$, $\mathbf{u}^{(1)} = (1/\sqrt{2})(1, 1)^T$, $\mathbf{v}^{(1)} = \sqrt{2}(p, 1-p)$, $\mathbf{u}^{(2)} = \sqrt{2}(1-p, -p)^T$, and $\mathbf{v}^{(2)} = (1/\sqrt{2})(1, -1)$. By substituting them in Eqs. (18) and (27) for $M=2$ and setting $\zeta_1 = \zeta_2 = 1/2$, we obtain

$$\mu_1 = \mu_2 = \frac{V_{11}}{2} + \left(1 - \frac{V_{11}}{2}\right) \frac{1-e^{-\kappa\tau}}{\kappa\tau}, \quad (31)$$

$$\mu_\Phi = \frac{V_{11}}{2} + \left(\frac{1}{2} - \frac{V_{11}}{2}\right) \frac{1-e^{-\kappa\tau}}{\kappa\tau}, \quad (32)$$

where $V_{11} = 2p^2 + 2(1-p)^2$. For any κ and τ values, the best precision is obtained in the symmetric case ($p=0.5$). Fig. 8 suggests that the analytical and numerical results are in strong agreement.

All-to-all coupling: The second example is all-to-all coupling; i.e., $w_{ij} = 1/N$ for $1 \leq i, j \leq N$. The eigenvalues are given by $\lambda_n = 1$ ($2 \leq n \leq N$). Because all the nodes are equivalent (i.e., permutation symmetry), we obtain $\mu_i = \langle \mu \rangle$. Then, from Eq. (20), it follows that

$$\mu_i = \frac{1}{N} + \left(1 - \frac{1}{N}\right) \frac{1-e^{-\kappa\tau}}{\kappa\tau}. \quad (33)$$

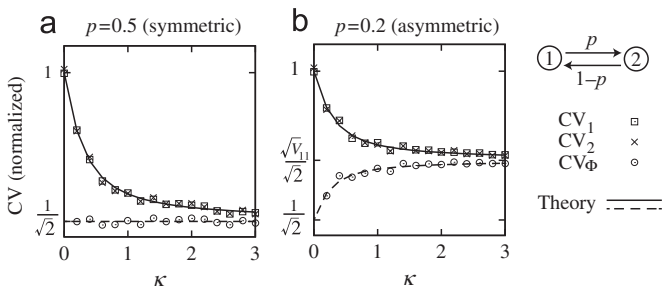


Fig. 8. Normalized CV versus coupling strength in asymmetrically coupled phase oscillators ($N=2$). Presented is the normalized CV, i.e., $CV_i/(\sqrt{D}\tau/2\pi)$ ($i = 1, 2$) and $CV_\Phi/(\sqrt{D}\tau/2\pi)$ for two coupled phase oscillators with (a) $p=0.5$ and (b) $p=0.2$. Numerical results are shown by symbols. The solid and dotted lines represent the analytical results given by Eqs. (31) and (32), respectively. Note that $V_{11} = 2p^2 + 2(1-p)^2 = 1$ for $p=0.5$ and $V_{11} = 1.36$ for $p=0.2$.

We also obtain a concise form for μ_Φ (see Appendix E), given by

$$\mu_\Phi = \frac{1}{N} + \left(\frac{1}{M} - \frac{1}{N}\right) \frac{1-e^{-\kappa\tau}}{\kappa\tau}. \quad (34)$$

We denote the CV value at $N=N^*$ by CV^* . By equating the first and second terms on the right-hand side in Eq. (34) and assuming $M \ll N$ and $e^{-\kappa\tau} \ll 1$, we obtain

$$N^* \approx \kappa\tau M, \quad CV^* \propto \frac{1}{\sqrt{\kappa\tau M}}. \quad (35)$$

Fig. 9 shows the analytical and numerical results. Note that in Figs. 4 and 5(b), the lower bounds are roughly proportional to $1/\sqrt{M}$, as our theory predicts.

Ring: The third example is the ring of size N , i.e., $w_{i,i+1} = w_{i-1,i} = 1/2$ for $1 \leq i \leq N$ and $w_{ij} = 0$ for $j \neq i-1, i+1$, as an example of spatially extended systems. For this network, we obtain

$$\lambda_n = 1 - \cos\left(\frac{2(n-1)\pi}{N}\right) \quad (36)$$

for $1 \leq n \leq N$. Because L is symmetric and the network has permutation symmetry, we obtain $\mu_i = \langle \mu \rangle$ where $\langle \mu \rangle$ is given by Eqs. (20) and (36). Fig. 10 shows the analytical and numerical results. Although each cell is adjacent to just two cells for any $N \geq 3$, there is a clear N -dependence of the CV for individual cells. Temporal precision is not simply determined by local connectivity.

The lower bound of the CV for the ring is considerably larger than that for the all-to-all network (Figs. 9(a) and 10). The reason for this is as follows. The Laplacian of the ring for a large N value has negligible eigenvalues (i.e., λ_n for $n \approx 0$ and $n \approx N$ in Eq. (36)), and these eigenvalues significantly enlarge the second term of

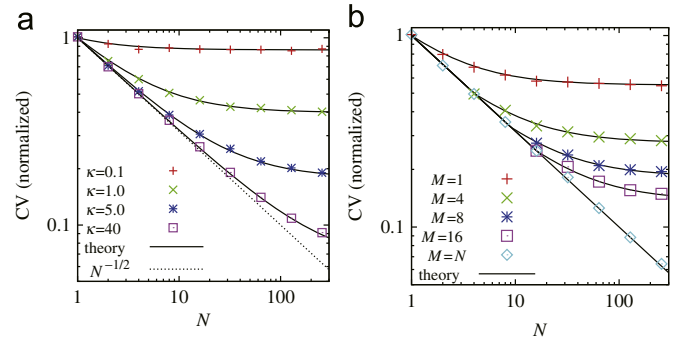


Fig. 9. Normalized CV in phase oscillators on the all-to-all network. (a) CV for individual cells ($M=1$) for various κ and N values. (b) CV for ensemble activity for various M values with $\kappa=0.5$. Symbols represent numerical data. Solid lines represent (a) $\sqrt{\mu_i}$ given by Eq. (33) and (b) $\sqrt{\mu_\Phi}$ given by Eq. (34).

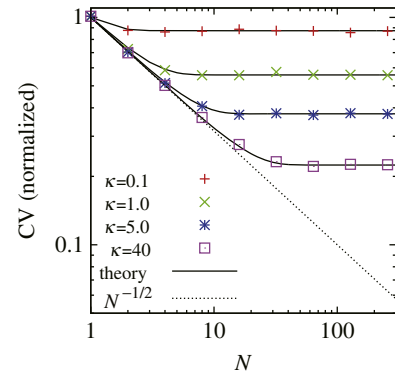


Fig. 10. Normalized CV for single cells in phase oscillators on the ring. Symbols represent numerical results. Solid lines represent $\sqrt{\mu_i}$ given by Eq. (20) with Eq. (36).

Eq. (20). In contrast, there is a nonvanishing spectrum gap (i.e., the second smallest eigenvalue λ_2) in the all-to-all and various random networks (Monasson, 1999; Samukhin et al., 2008). In the FHN model, we observed a similar difference between the cases of the square lattice (Fig. 3(b)) and the all-to-all and random networks (Fig. 3(a) and (c), respectively). This is also because the square lattice has negligible eigenvalues (Mohar, 1991). Such small eigenvalues are associated with slow synchronization of remote oscillators owing to a time lag in communication, and this property is shared by any spatially extended networks with local interaction. Therefore, spatial networks with only local interaction are disadvantageous to temporal precision.

Small-world networks: By using a type of the Watts–Strogatz model (Newman, 2000; Newman et al., 2000) of fixed size N , we demonstrate that a small fraction of long-range interactions added to the ring drastically improves temporal precision. We generate a network by adding pN bidirectional shortcuts sequentially to the ring, where p is the shortcut density. Under the condition that multiple links are avoided, the two endpoints of each shortcut are chosen from the N nodes with equal probability. The generated network is undirected. To maintain the total coupling strength independent of p , we set $w_{ij} = w_{ji} = 1/(2+2p)$ for all links. The ring and all-to-all networks are obtained at $p=0$ and $p=N/2-1$, respectively. Fig. 11 shows the numerically obtained $\langle CV \rangle$ for each p , where $\langle CV \rangle \equiv \sum_{i=1}^N CV_i/N$ for a single realization of the network. The lines represent $\sqrt{\langle \mu \rangle}$ obtained from Eq. (20), where we numerically computed the eigenvalues λ_n for the generated network. We set the coupling strength such that $\langle \mu \rangle \gg 1/N$ (i.e., $N \gg N^*$) for the initial ring ($p=0$).

Fig. 11 indicates that temporal precision is considerably improved at $p \approx 1$, i.e., when $O(N)$ shortcuts are added (the small-world regime). Moreover, the corresponding CV value is close to that of the all-to-all network, in which $O(N^2)$ “shortcuts” exist. As discussed above, there are small eigenvalues that hamper temporal precision in spatially extended networks. Such small eigenvalues do not exist in networks with a sufficient number of shortcuts because of rapid communication between any pair of oscillators.

3.5. Mechanism of the crossover

We demonstrated using various models that the crossover generally occurs in the collective enhancement. On the basis of our theory, the crossover can be interpreted as follows. When Jacobian L is symmetric, the SD for the mean phase decreases as $1/\sqrt{N}$ for any N (Eq. (28)). When coupling strength κ is infinite, the oscillators are completely synchronized in phase. Then, the phase of each oscillator is identical with the mean phase, and so is the SD, i.e., $SD_i \propto 1/\sqrt{N}$ for any N . This behavior is expressed in the first term on the right-hand side of Eq. (19). However, for finite κ ,

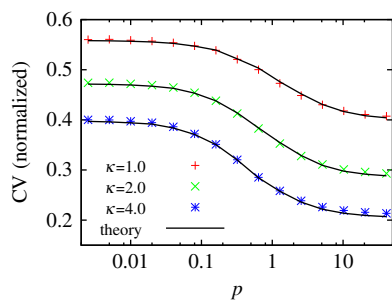


Fig. 11. Normalized CV for individual cells in phase oscillators on the variant of the Watts–Strogatz model. We present $\langle CV_i \rangle / (\sqrt{\tau D} / 2\pi)$, where $\langle CV_i \rangle \equiv \sum_{i=1}^N CV_i/N$. Lines represent $\sqrt{\langle \mu \rangle}$ given by Eq. (19). We set $N=400$.

individual oscillators’ phases fluctuate around the mean phase because of the independent noise applied to the oscillators. Owing to this additional fluctuation, the SD for individual oscillators is larger than that for the mean phase, as expressed in the second term on the right-hand side of Eq. (19). Although the fluctuation in the mean phase vanishes with the limit $N \rightarrow \infty$, it remains finite in individual oscillators. This is the origin of the lower bound.

In our previous paper (Masuda et al., 2010), with Eq. (3), we analyzed phase diffusion after infinitely many cycles. There, we neglected the second term on the right-hand side of Eq. (18) because we assumed that λ_2 is nonvanishing and a period of infinitely many cycles corresponds to $\tau \rightarrow \infty$. In contrast, the temporal precision defined in the present paper is based on cycle-to-cycle periods, so that we need to consider finite τ . The second term can be comparable to or even larger than the first term for large N or small κ values. Particularly in these cases, our extension from the previous paper (Masuda et al., 2010) is crucial for the understanding of temporal precision. It should also be noted that our theory in the present paper can be applied to the case of infinitely small λ_2 , as is the case in, e.g., the ring with large N values (see Eq. (36)).

3.6. Relation between synchrony and temporal precision

With the example shown in Fig. 3(d), we demonstrated that temporal precision is enhanced as N increases while the level of synchrony is unchanged (Fig. 3(d)). This example implies that synchrony and temporal precision are distinct properties of oscillator networks.

The level of synchrony is estimated by the proximity of the state in the phase to the synchronized state. The level of synchrony generally increases with eigenvalues $\kappa \lambda_n$ ($n \geq 2$) because then the synchronized state is more strongly attracting. The noise scaling factor for symmetric L has the same tendency; i.e., the second term of the right-hand side in Eq. (20) also decreases with eigenvalues $\kappa \lambda_n$ ($n \geq 2$). However, the first term in Eq. (20) depends only on N and has nothing to do with the level of synchrony, as is obvious from the fact that this term is independent of coupling strength κ . This term makes temporal precision distinct from synchrony.

4. Discussion and conclusions

We found that the collective enhancement is ineffective for system size N above the crossover point N^* . We further showed that N^* increases with coupling strength (Eq. (23)). Therefore, as oscillators are more strongly coupled, the behavior $CV \propto 1/\sqrt{N}$ persists up to a larger N value. This is the case for different oscillation and coupling mechanisms, as demonstrated in the two biological models (the FHN and SCN models) and the phase oscillator model. Moreover, this behavior also holds true for different network connectivities, as demonstrated using the ring, the square lattice, the all-to-all network, and the random graph.

Our theory is useful for inferring the magnitude of fluctuations in individual cells and the coupling strength between cells. Suppose that temporal precision in a pacemaker tissue that is genetically modified or subjected to a treatment (e.g., drug) is lower than that in an intact tissue. If the cells in the tissue are well synchronized in both cases, one may consider that the treatment affects the oscillation mechanism of individual cells. Our theory suggests another possibility: a decrease in the coupling strength, not the alteration in the oscillation property of individual cells, may be the reason for the reduced temporal precision (Fig. 3(a,b,c)). By observing reduced temporal precision

only, we cannot distinguish these two possibilities. However, our theory makes it possible to individually quantify the effects of the treatment on the two properties if we can observe cell networks of different sizes. By observing temporal precision in small (*i.e.*, $N < N^*$) tissues of different sizes, we can infer the magnitude of fluctuations in individual cells by fitting the law $CV \propto 1/\sqrt{N}$. Furthermore, by observing relatively large tissues and determining N^* values for different treatments (*e.g.*, different days of cultivation, different concentrations of a drug, treated versus untreated), we can infer changes in the coupling strength induced by the treatment because N^* increases with the coupling strength (Eq. (23)).

Our study also indicates that long-range interactions among cells are advantageous to temporal precision. As demonstrated in Fig. 11, the addition of shortcut links considerably decreases the CV. A similar result was reported in a previous numerical study using a more realistic model for the SCN (Vasalou et al., 2009). This result might underlie an evolutionary origin of dense fibers across the SCN (Abrahamson and Moore, 2001).

Our theoretical results provide an interpretation of previous experiments on cardiac and circadian oscillations. Kojima et al. (2006) observed a decrease in the CV with increasing cell number in cultivated cardiac cells coupled via micro channels. They showed that the CV decreases considerably with N for small N values ($N=1,2,3$), while it is almost constant for $N \geq 4$. In contrast, in cultivated cardiac cells that are directly and tightly coupled to each other, Clay and DeHaan (1979) found that the reduction in the CV roughly obeys $CV \propto 1/\sqrt{N}$ up to $N \approx 100$. Although the cells are kept synchronized in both cases, the behavior of temporal precision is different. This discrepancy may be due to a difference in coupling strength. While the coupling was strong enough to guarantee synchrony in both cases, coupling in the latter experiments may be stronger than that in the former experiments, resulting in $N^* \approx 4$ and $N^* > 100$, respectively. It would be of great interest to investigate systematically how the crossover point increases with coupling strength, possibly controlled by the width of the micro channel implemented in the former experiments (Kojima et al., 2006).

Collective enhancement has been examined experimentally in circadian oscillation as well. Herzog et al. (2004) measured temporal precision in SCN cells. There, individual cell oscillations in both synchronized and unsynchronized cases were observed in slice cultures of SCN and dispersed SCN cells, respectively. They found that the SD in the former (0.42 h) was approximately five times smaller than that in the latter (2.1 h), and argued that the collective enhancement of temporal precision occurs in synchronized cells. They further speculated that, under the assumption $SD \approx 1/\sqrt{N}$, only 25 cells out of the order of 10^5 cells composing the SCN are involved in the collective enhancement of temporal precision in the explant SCN.

We interpret this experimental result as follows. In the SCN, a wave pattern is observed (Yamaguchi et al., 2003; Doi et al., 2011). As indicated above as well as in our previous paper (Masuda et al., 2010), the law $SD \propto 1/\sqrt{N}$ is violated in the presence of a wave pattern even if the coupling is sufficiently strong. Roughly speaking, the reason for this is that only the cells forming the source of the wave pattern can contribute to the collective enhancement of temporal precision, and other cells simply obey those cells (Masuda et al., 2010). The number of cells forming the source might be of the order of 25. Cells located downstream of the wave may contribute to functions other than temporal precision.

In our theoretical approach, we assumed that all oscillators are synchronized in frequency. We expect that this is a reasonable approximation for biological systems. For example, in the slice culture of the SCN, most of observed cells appear to be well

synchronized in frequency (Yamaguchi et al., 2003; Doi et al., 2011). In the heart, most cells are thought to be synchronized in frequency because otherwise spiral waves may arise and those waves are associated with pathological behavior such as tachycardia and fibrillation (Winfree, 2001).

Our approach can not be applied to the case of partial synchronization, where a large number of oscillators are not synchronized in frequency. It is of great interest to extend our theory to partial synchronization. However, an established analytical method to treat partial synchronization works only for the all-to-all network of infinite system size (Ott and Antonsen, 2008, 2009; Kawamura et al., 2010), while we are concerned with general networks of finite system size. Therefore, we leave it as an open problem.

Our theory is widely applicable to frequency-synchronized oscillators with weak noise and weak coupling. Our theory can also apply to the case of the coexistence of multiple coupling mechanisms, only by replacing coupling function f by f_{ij} in the phase model (Eq. (3)). Although the phase model is not justified when the assumption of weak noise and weak coupling is violated, we have numerically confirmed that our main finding, *i.e.*, the properties (i)–(v), are preserved in the case of strong coupling and strong noise (Fig. 5). We thus expect that our theory, based on the phase model, captures the essence of the collective enhancement of temporal precision.

Acknowledgments

The authors are grateful for fruitful discussions with Erik Herzog, István Z. Kiss, Steven Strogatz, and Ikuro Suzuki. N.M. acknowledges the support provided through Grants-in-Aid for Scientific Research (No. 23681033, and Innovative Areas “Systems Molecular Ethology” (No. 20115009)) from MEXT, Japan.

Appendix A. Definition of models and networks

We consider two systems—the FHN model and the SCN model representing the cardiac pacemaker organ and the circadian master clock, respectively.

The FHN model has been extensively used as a model of neurons and cardiac cells (Keener and Sneyd, 1998). Our FHN model is given by

$$\frac{dx_i}{dt} = x_i(a - x_i)(x_i - 1) - y_i + \rho \xi_i(t) + \kappa \sum_{j=1}^N A_{ij}(x_j - x_i), \quad (37a)$$

$$\frac{dy_i}{dt} = \epsilon(x_i - by_i + c), \quad (37b)$$

where a, b, c, ϵ are the model parameters, ρ is the noise strength, $\xi_i(t)$ is white Gaussian noise with $E[\xi_i(t)] = 0$ and $E[\xi_i(t)\xi_j(t')] = \delta_{ij}\delta(t - t')$. We chose parameter values such that each unit is autonomous oscillator. In Figs. 1, 3 and 4, we set $a = 0.1, \epsilon = 0.01, b = 0.5$, and $c = 0.05$. In Fig. 5(a), we replace c with $c_i = 0.1 + 0.02v_i$ ($1 \leq i \leq N$), where v_i is a random variable independently taken from the Gaussian distribution with zero mean and unit variance. We varied the noise strength and coupling strength, as specified in the figures and their captions. The distance δ from the in-phase state is defined as

$$\delta = \sqrt{\frac{1}{N-1} \sum_{i=1}^N (x_i - \bar{x})^2}, \quad (38)$$

where $\bar{x} = \sum_{i=1}^N x_i / N$.

As the SCN model, we employed a previously proposed model (Locke et al., 2008), given by

$$\frac{dx_i}{dt} = T_i \left(V_1 \frac{K_1^n}{K_1^n + z_i^n} - V_2 \frac{x_i}{K_2 + x_i} + V_c \frac{\kappa F_i}{K_c + \kappa F_i} \right) + \rho \zeta_i^{(x)}, \quad (39a)$$

$$\frac{dy_i}{dt} = T_i \left(k_3 x_i - V_4 \frac{y_i}{K_4 + y_i} \right) + \rho \zeta_i^{(y)}, \quad (39b)$$

$$\frac{dz_i}{dt} = T_i \left(k_5 y_i - V_6 \frac{z_i}{K_6 + z_i} \right) + \rho \zeta_i^{(z)}, \quad (39c)$$

$$\frac{dr_i}{dt} = T_i \left(k_7 x_i - V_8 \frac{r_i}{K_8 + r_i} \right) + \rho \zeta_i^{(r)}, \quad (39d)$$

$$F_i = \sum_{j=1}^N A_{ij} r_j, \quad (39e)$$

where $V_1 = 6.8355$, $n = 5.6645$, $K_1 = 2.7266$, $K_2 = 0.2910$, $k_3 = 0.1177$, $V_4 = 1.0841$, $K_4 = 8.1343$, $k_5 = 0.3352$, $V_6 = 4.6645$, $K_6 = 9.9849$, $k_7 = 0.2282$, $V_8 = 3.5216$, $K_8 = 7.4519$, $V_c = 6.7924$, $K_c = 4.8283$, $\kappa = 12.0$, and $V_2 = 12.0$. All parameter values except for κ and V_2 are taken from (Locke et al., 2008). Time constant T_i is introduced to express heterogeneity in the oscillation period. We set $T_i = 1$ in Fig. 1. In Fig. 5(b), $T_i = 1 + 0.05v_i$ with v_i independently obeying the Gaussian distribution with zero mean and unit variance. The functions $\zeta_i^{(\zeta)}(t)$ ($\zeta = x, y, z, r$) represent white Gaussian noise processes with $E[\zeta_i^{(\zeta)}(t)] = 0$ and $E[\zeta_i^{(\zeta)}(t)\zeta_j^{(\zeta)}(t')] = \delta_{ij}\delta_{\zeta\eta}\delta(t-t')$. The noise strength ρ and coupling strength κ are specified in the figures and their captions.

In both models, we applied sufficiently strong coupling to ensure that the oscillators were synchronized nearly in phase. When we computed the CV, we assumed random initial conditions and measured a sufficiently large number of cycle-to-cycle periods after the transient.

The all-to-all network used in Figs. 1(b,d,f), 3(a,d), 4, 5(b) and 9 is defined by $A_{ij} = 1/N$ for $1 \leq i, j \leq N$. The one-dimensional lattice with an open boundary condition used in Fig. 1(e) is defined by $A_{ij} = 1/2$ for $1 \leq i \leq N$ and $1 \leq j = i \pm 1 \leq N$, and $A_{ij} = 0$ otherwise. The ring used in Fig. 10 is the same as the one-dimensional lattice except that we impose a periodic boundary condition $A_{1,N} = A_{N,1} = 1/2$. The square lattice with an open boundary condition used in Figs. 3(b) and 5(a) is defined by $A_{ij} = 1/4$ with cell j adjacent to i for $1 \leq i, j \leq \sqrt{N}$ and $A_{ij} = 0$ otherwise. The undirected random graph used in Fig. 3(c) is the Erdős–Rényi random graph, where $A_{ij} = A_{ji} = 1/8$ for $1 \leq i < j \leq N$ with probability $p = 8/N$ and $A_{ij} = A_{ji} = 0$ otherwise. We set link weights such that the summed weight of the links per node is independent of N ; i.e., for $1 \leq i \leq N$, $\sum_{j=1}^N A_{ij} = 1$ in the ring and all-to-all network and $\sum_{j=1}^N A_{ij} \approx 1$ in the other networks including the Watts–Strogatz model used in Fig. 11.

Appendix B. Phase description

A large class of oscillator systems including the FHN and SCN models (Eqs. (37) and (39)) are reduced to phase models if the coupling and noise are sufficiently weak (Winfree, 1967; Kuramoto, 1984). The concept behind the reduction is as follows. We denote an element of the state variable of the i th oscillator by $x_i(t)$. When unperturbed, the oscillator portrays a one-dimensional closed orbit after transient so that $x_i(t) = x_i(t + 2\pi/\omega_i)$, where ω_i is the intrinsic frequency. We define the phase ϕ_i by $x_i(t) = x_i(\phi_i/\omega_i)$; that is, the phase increases linearly with time in the unperturbed oscillator. For convenience, we denote the unperturbed orbit by $\chi(\phi_i) = x_i(\phi_i/\omega_i)$. Although the trajectory deviates from the closed orbit when the oscillator is weakly perturbed, it is still possible to parametrize a trajectory of an

oscillator by only the phase and describe the dynamics of coupled oscillators in terms of the phases only (Winfree, 1967; Kuramoto, 1984). The resulting equation is given by Eq. (3). Because of the assumption of weak perturbation, $x_i(t)$ is approximated by that of the unperturbed orbit, i.e.,

$$x_i(t) \approx \chi(\phi_i(t)). \quad (40)$$

Therefore, the first passage time problem for $x_i(t)$ is approximated by that for $\phi_i(t)$.

Appendix C. Calculation of Eq. (18)

Our linearized equation is given by Eq. (14), which is reproduced as

$$\dot{\theta}_i(t) = -\kappa \sum_{j=1}^N L_{ij} \theta_j + \sqrt{D} \zeta_i(t), \quad (41)$$

where θ_i ($1 \leq i \leq N$) is the deviation from the synchronized state, $\kappa > 0$ is the coupling strength, $L = (L_{ij})$ is a diagonalizable matrix, and $\zeta_i(t)$ is white Gaussian noise with

$$E[\zeta_i(t)] = 0, \quad E[\zeta_i(t)\zeta_j(s)] = \delta_{ij}\delta(t-s). \quad (42)$$

From the assumption of the stability of frequency synchronization, we have

$$0 = \lambda_1 < \text{Re } \lambda_2 \leq \text{Re } \lambda_3 \leq \dots \leq \text{Re } \lambda_N. \quad (43)$$

The right and left eigenvectors of L corresponding to λ_n are denoted by $\mathbf{u}^{(n)} = (u_i^{(n)})$ and $\mathbf{v}^{(n)} = (v_i^{(n)})$, respectively; i.e.,

$$L\mathbf{u}^{(n)} = \lambda_n \mathbf{u}^{(n)}, \quad (44a)$$

$$\mathbf{v}^{(n)}L = \lambda_n \mathbf{v}^{(n)} \quad (44b)$$

with the normalization and orthogonality conditions

$$\mathbf{v}^{(m)}\mathbf{u}^{(n)} = \delta_{mn}. \quad (45)$$

Using these eigenvectors, we decompose $\theta_i(t)$ as

$$\theta_i(t) = \sum_{m=1}^N \varphi_m(t) \mathbf{u}_i^{(m)}, \quad (46)$$

where $\varphi_m(t)$ is given by

$$\varphi_m(t) = \sum_{i=1}^N \theta_i(t) v_i^{(m)}. \quad (47)$$

By taking the time derivative of Eq. (47) and using Eqs. (41), (45) and (46), we obtain

$$\dot{\varphi}_m(t) = -\kappa \lambda_m \varphi_m + \eta_m(t), \quad (48)$$

where

$$\eta_m(t) = \sqrt{D} \sum_{i=1}^N v_i^{(m)} \zeta_i(t). \quad (49)$$

Eq. (42) yields $\langle \eta_m(t) \rangle = 0$. We also have

$$\begin{aligned} E[\eta_m(t)\eta_n(s)] &= E \left[D \sum_{i=1}^N v_i^{(m)} \zeta_i(t) \sum_{j=1}^N v_j^{(n)} \zeta_j(s) \right] \\ &= D \sum_{i,j=1}^N v_i^{(m)} v_j^{(n)} E[\zeta_i(t)\zeta_j(s)] = D \sum_{i,j=1}^N v_i^{(m)} v_j^{(n)} \delta_{ij}\delta(t-s) \\ &= D \left(\sum_{i=1}^N v_i^{(m)} v_i^{(n)} \right) \delta(t-s) = DV_{mn} \delta(t-s), \end{aligned} \quad (50)$$

where

$$V_{mn} \equiv \sum_{i=1}^N v_i^{(m)} v_i^{(n)}. \quad (51)$$

Now we derive C_{ij} given in Eq. (18). The definition of C_{ij} is

$$C_{ij} \equiv \frac{1}{D\tau} E[(\theta_i(t+\tau) - \theta_i(t))(\theta_j(t+\tau) - \theta_j(t))]. \quad (52)$$

By substituting Eq. (46) in Eq. (52), we obtain

$$C_{ij} = \frac{1}{D\tau} \sum_{m,n=1}^N u_i^{(m)} u_j^{(n)} E[(\varphi_m(t+\tau) - \varphi_m(t))(\varphi_n(t+\tau) - \varphi_n(t))]. \quad (53)$$

The solution to Eq. (48) is formally written as

$$\varphi_m(t) = e^{-\kappa\lambda_m t} \varphi_m(0) + \int_0^t ds e^{-\kappa\lambda_m(t-s)} \eta_m(s). \quad (54)$$

Using Eq. (54), we obtain

$$\varphi_1(t+\tau) - \varphi_1(t) = \int_t^{t+\tau} ds \eta_1(s), \quad (55)$$

$$\begin{aligned} E[(\varphi_1(t+\tau) - \varphi_1(t))(\varphi_1(t+\tau) - \varphi_1(t))] &= \int_t^{t+\tau} ds_1 \int_t^{t+\tau} ds_2 E[\eta_1(s_1)\eta_1(s_2)] \\ &= DV_{11} \int_t^{t+\tau} ds_1 \int_t^{t+\tau} ds_2 \delta(s_1 - s_2) = DV_{11} \tau. \end{aligned} \quad (56)$$

To evaluate the terms on the right-hand side of Eq. (53) for $m+n > 2$, we first calculate

$$\begin{aligned} B_{mn}(t_1, t_2) &\equiv \int_0^{t_1} ds_1 \int_0^{t_2} ds_2 e^{-\kappa\lambda_m(t_1-s_1) - \kappa\lambda_n(t_2-s_2)} E[\eta_m(s_1)\eta_n(s_2)] \\ &= \int_0^{t_1} ds_1 \int_0^{t_2} ds_2 e^{-\kappa\lambda_m(t_1-s_1) - \kappa\lambda_n(t_2-s_2)} DV_{mn} \delta(s_1 - s_2) \\ &= DV_{mn} \int_0^{\min(t_1, t_2)} ds e^{-\kappa\lambda_m(t_1-s) - \kappa\lambda_n(t_2-s)} \\ &\rightarrow DV_{mn} \frac{e^{-\kappa\lambda_m(t_1-s) - \kappa\lambda_n(t_2-s)}}{\kappa(\lambda_m + \lambda_n)} \Big|_{s=\min(t_1, t_2)}. \end{aligned} \quad (57)$$

We consider the limit $t \rightarrow \infty$ in Eq. (57) because we are concerned with a stationary process. Using Eq. (57), we obtain

$$\begin{aligned} E[(\varphi_m(t+\tau) - \varphi_m(t))(\varphi_n(t+\tau) - \varphi_n(t))] &= B_{mn}(t+\tau, t+\tau) - B_{mn}(t+\tau, t) - B_{mn}(t, t+\tau) + B_{mn}(t, t) \\ &\rightarrow DV_{mn} \frac{2 - e^{-\kappa\lambda_m \tau} - e^{-\kappa\lambda_n \tau}}{\kappa(\lambda_m + \lambda_n)} \quad (t \rightarrow \infty). \end{aligned} \quad (58)$$

By combining Eqs. (53), (56) and (58), we obtain

$$C_{ij} = V_{11} u_i^{(1)} u_j^{(1)} + \sum_{m,n(m+n>2)} \frac{2 - e^{-\kappa\lambda_m \tau} - e^{-\kappa\lambda_n \tau}}{\kappa(\lambda_m + \lambda_n) \tau} V_{mn} u_i^{(m)} u_j^{(n)}. \quad (59)$$

In Eq. (18), we set $u_i^{(1)} = 1/\sqrt{N}$ for $1 \leq i \leq N$.

Appendix D. Scaling factor μ_ϕ for the ensemble activity

In this section, we derive μ_ϕ used in Eqs. (28) and (29). By substituting Eq. (40) in Eq. (24), we express the ensemble activity $X(t)$ in terms of the phases as

$$X(t) = \sum_{i=1}^M \zeta_i x_i(t) \approx \sum_{i=1}^M \zeta_i \chi(\phi_i(t)). \quad (60)$$

For in-phase synchrony (i.e., $\psi_i = 0$) and small deviation θ_i , we can further approximate $X(t)$ to

$$X(t) \approx \chi(\Omega t) + \sum_{i=1}^M \zeta_i \chi'(\Omega t) \theta_i(t) \approx \chi(\Phi(t)), \quad (61)$$

where $\chi'(\phi) = d\chi(\phi)/d\phi$ and Φ is the mean phase of the ensemble, given by

$$\Phi(t) = \Omega t + \sum_{i=1}^M \zeta_i \theta_i(t). \quad (62)$$

Thus, similar to the case of individual cell oscillations, the cycle-to-cycle period for the ensemble activity $X(t)$ is approximated by the cycle-to-cycle period $\Delta t_\phi^{(k)}$ for the mean phase $\Phi(t)$. We further employ the following approximation (Fig. 7):

$$\frac{2\pi}{\tau} \text{std}[\Delta t_\phi] \approx \text{std}[\Delta \Phi], \quad (63)$$

where $\Delta \Phi \equiv \Phi(t+\tau) - \Phi(t) - 2\pi$. We define the scaling factor μ_ϕ for the ensemble activity as

$$\text{var}[\Delta \Phi] = \mu_\phi D\tau. \quad (64)$$

We then obtain

$$\begin{aligned} \mu_\phi &= \frac{\text{var}[\Delta \Phi]}{D\tau} = \sum_{i,j=1}^M \zeta_i \zeta_j \frac{E[(\theta_i(t+\tau) - \theta_i(t))(\theta_j(t+\tau) - \theta_j(t))]}{D\tau} \\ &= \sum_{i,j=1}^M \zeta_i \zeta_j C_{ij}, \end{aligned} \quad (65)$$

where C_{ij} is given by Eq. (18).

We consider the case of symmetric L and $\zeta_i = 1/M$ for $1 \leq i \leq M$. Substituting Eq. (19) in Eq. (65), we obtain

$$\mu_\phi = \frac{1}{N} + \frac{1}{M^2} \sum_{n=2}^N \sum_{i,j=1}^M \frac{1 - e^{-\kappa\lambda_n \tau}}{\kappa\lambda_n \tau} u_i^{(n)} u_j^{(n)}. \quad (66)$$

For $M=N$, $\sum_{i=1}^N u_i^{(n)} = \mathbf{u}^{(1)} \cdot \mathbf{u}^{(n)} = 0$ for $2 \leq n \leq N$ (orthogonality) leads to

$$\mu_\phi = \frac{1}{N}, \quad (67)$$

that is, there is no crossover. For $M < N$, Eq. (66) implies that μ_ϕ depends on the choice of M oscillators. When we randomly choose M out of N oscillators, where $1 \ll M \ll N$, the dependence of μ_ϕ on M is estimated as follows. The orthogonality and normalization, respectively, imply

$$\frac{1}{N} \sum_{i=1}^N u_i^{(n)} = 0, \quad \frac{1}{N} \sum_{i=1}^N u_i^{(n)} u_i^{(n)} = \frac{1}{N}. \quad (68)$$

Therefore, the distribution of $u_i^{(n)}$ ($1 \leq i \leq N$) has the mean of 0 and variance of $1/N$. We randomly choose M ($\ll N$) elements and assume that they are independent random numbers with the same mean and variance. Then, we apply the central limit theorem for $M \gg 1$ to obtain

$$\sum_{i=1}^M \sum_{j=1}^M u_i^{(n)} u_j^{(n)} \approx \sum_{i=1}^M u_i^{(n)} u_i^{(n)} \approx \frac{M}{N}. \quad (69)$$

By substituting Eq. (69) in the right-hand side of Eq. (66), we obtain Eq. (29).

Appendix E. Calculation of Eq. (34)

It is convenient to choose the eigenvectors $\mathbf{u}^{(n)} = (u_i^{(n)})$ for $2 \leq n \leq N$ as $u_i^{(n)} = 1/\sqrt{n^2-n}$ for $1 \leq i \leq n-1$, $u_n^{(n)} = (1-n)/\sqrt{n^2-n}$ and $u_i^{(n)} = 0$ for $n \leq i \leq N$. Then, the following property holds:

$$\frac{1}{M} \sum_{i=1}^M u_i^{(n)} = \begin{cases} 0 & \text{for } 2 \leq n \leq M, \\ \frac{1}{\sqrt{n^2-n}} & \text{for } M+1 \leq n \leq N. \end{cases} \quad (70)$$

Substitution of Eq. (70) and the eigenvalues $\lambda_n = 1$ ($2 \leq n \leq N$) in Eq. (66) results in

$$\begin{aligned} \mu_\phi &= \frac{1}{N} + \frac{1-e^{-\kappa\tau}}{\kappa\tau} \sum_{n=2}^N \left(\frac{1}{M} \sum_{i=1}^M u_i^{(n)} \right) \left(\frac{1}{M} \sum_{j=1}^M u_j^{(n)} \right) \\ &= \frac{1}{N} + \frac{1-e^{-\kappa\tau}}{\kappa\tau} \sum_{n=M+1}^N \frac{1}{n^2-n} = \frac{1}{N} + \frac{1-e^{-\kappa\tau}}{\kappa\tau} \sum_{n=M+1}^N \left(\frac{1}{n-1} - \frac{1}{n} \right) \\ &= \frac{1}{N} + \left(\frac{1}{M} - \frac{1}{N} \right) \frac{1-e^{-\kappa\tau}}{\kappa\tau}. \end{aligned} \quad (71)$$

References

- Abrahamson, E.E., Moore, R.Y., 2001. Suprachiasmatic nucleus in the mouse: retinal innervation, intrinsic organization and efferent projections. *Brain Res.* 916, 172–191.
- Agave, R., Chebotarev, P., 2000. The matrix of maximum out forests of a digraph and its applications. *Autom. Remote Control* 61, 1424–1450.
- Arenas, A., Diaz-Guilera, A., Kurths, J., Moreno, Y., Zhou, C., 2008. Synchronization in complex networks. *Phys. Rep.* 469, 93–153.
- Blasius, B., Tönjes, R., 2005. Quasiregular concentric waves in heterogeneous lattices of coupled oscillators. *Phys. Rev. Lett.* 95 (8), 84101.
- Clay, J.R., DeHaan, R.L., 1979. Fluctuations in interbeat interval in rhythmic heart-cell clusters. Role of membrane voltage noise. *Biophys. J.* 28 (3), 377–389.
- Doi, M., Ishida, A., Miyake, A., Sato, M., Komatsu, R., Yamazaki, F., Kimura, I., Tsuchiya, S., Kori, H., Seo, K., Yamaguchi, Y., Matsuo, M., Fustin, J.-M., Tanaka, R., Santo, Y., Yamada, H., Takahashi, Y., Araki, M., Nakao, K., Aizawa, S., Kobayashi, M., Obrietan, K., Tsujimoto, G., Okamura, H., 2011. Circadian regulation of intracellular g-protein signalling mediates intercellular synchrony and rhythmicity in the suprachiasmatic nucleus. *Nat. Commun.* 2, 327.
- Enright, J.T., 1980. Temporal precision in circadian systems: a reliable neuronal clock from unreliable components? *Science* 209, 1542–1545.
- Ermentrout, G., 1992. Stable periodic solutions to discrete and continuum arrays of weakly coupled nonlinear oscillators. *SIAM J. Appl. Math.* 52 (6), 1665.
- Garcia-Ojalvo, J., Elowitz, M.B., Strogatz, S.H., 2004. Modeling a synthetic multicellular clock: repressilators coupled by quorum sensing. *Proc. Natl. Acad. Sci.* 101, 10955–10960.
- Gerstner, W., Kistler, W., 2002. *Spiking Neuron Models: Single Neurons, Populations, Plasticity*. Cambridge University Press, Cambridge.
- Glass, L., 2001. Synchronization and rhythmic processes in physiology. *Nature* 410, 277–284.
- Heiligenberg, W., Finger, T., Matsubara, J., Carr, C., 1981. Input to the medullary pacemaker nucleus in the weakly electric fish, *eigenmannia* (sternopygidae, gymnotiformes). *Brain Res.* 211 (2), 418–423.
- Herzog, E.D., Aton, S.J., Numano, R., Sakaki, Y., Tei, H., 2004. Temporal precision in the mammalian circadian system: a reliable clock from less reliable neurons. *J. Biol. Rhythms* 19, 35–46.
- Honma, S., Shirakawa, T., Katsuno, Y., Namihira, M., Honma, K., 1998. Circadian periods of single suprachiasmatic neurons in rats. *Neurosci. Lett.* 250 (3), 157–160.
- Kawamura, Y., Nakao, H., Arai, K., Kori, H., Kuramoto, Y., 2010. Phase synchronization between collective rhythms of globally coupled oscillator groups: noiseless non-identical case. *Chaos* 20, 043110.
- Keener, J., Sneyd, J., 1998. *Mathematical Physiology*. Springer-Verlag, New York.
- Kojima, K., Kaneko, T., Yasuda, K., 2006. Role of the community effect of cardiomyocyte in the entrainment and reestablishment of stable beating rhythms. *Biochem. Biophys. Res. Commun.* 351 (1), 209–215.
- Kuramoto, Y., 1984. *Chemical Oscillations, Waves, and Turbulence*. Springer, New York.
- Locke, J., Westermark, P., Kramer, A., Herzog, H., 2008. Global parameter search reveals design principles of the mammalian circadian clock. *BMC Syst. Biol.* 2 (1), 22.
- Ly, C., Ermentrout, G., 2010. Coupling regularizes individual units in noisy populations. *Phys. Rev. E* 81 (1), 011911.
- Masuda, N., Kawamura, Y., Kori, H., 2010. Collective fluctuations in networks of noisy components. *New J. Phys.* 12, 093007.
- Mohar, B., 1991. The Laplacian spectrum of graphs. *Graph Theory Combinatorics Appl.* 2, 871–898.
- Monasson, R., 1999. Diffusion, localization and dispersion relations on “small-world” lattices. *Eur. Phys. J. B* 12 (4), 555–567.
- Moortgat, K., Bullock, T., Sejnowski, T., 2000a. Gap junction effects on precision and frequency of a model pacemaker network. *J. Neurophysiol.* 83 (2), 984–997.
- Moortgat, K.T., Bullock, T.H., Sejnowski, T.J., 2000b. Precision of the pacemaker nucleus in a weakly electric fish: network versus cellular influences. *J. Neurophysiol.* 83 (2), 971–983.
- Needleman, D.J., Tiesinga, P.H.E., Sejnowski, T.J., 2001. Collective enhancement of precision in networks of coupled oscillators. *Physica D* 155, 324–336.
- Newman, M., 2000. Models of the small world. *J. Statist. Phys.* 101 (3), 819–841.
- Newman, M., 2010. *Networks: An Introduction*. Oxford University Press, Oxford.
- Newman, M., Moore, C., Watts, D., 2000. Mean-field solution of the small-world network model. *Phys. Rev. Lett.* 84 (14), 3201–3204.
- Ott, E., Antonsen, T., 2009. Long time evolution of phase oscillator systems. *Chaos* 19, 023117.
- Ott, E., Antonsen, T.M., 2008. Low dimensional behavior of large systems of globally coupled oscillators. *Chaos* 18, 037113.
- Pecora, L., Carroll, T., 1998. Master stability functions for synchronized coupled systems. *Phys. Rev. Lett.* 80 (10), 2109–2112.
- Rappel, W., Karma, A., 1996. Noise-induced coherence in neural networks. *Phys. Rev. Lett.* 77 (15), 3256–3259.
- Reppert, S.M., Weaver, D.R., 2002. Coordination of circadian timing in mammals. *Nature* 418, 935–941.
- Samukhin, A., Dorogovtsev, S., Mendes, J., 2008. Laplacian spectra of, and random walks on, complex networks: Are scale-free architectures really important? *Phys. Rev. E* 77 (3), 036115.
- Sherman, A., Rinzel, J., Keizer, J., 1988. Emergence of organized bursting in clusters of pancreatic beta-cells by channel sharing. *Biophys. J.* 54 (3), 411–425.
- Tabareau, N., Slotine, J., Pham, Q., 2010. How synchronization protects from noise. *PLoS Comput. Biol.* 6 (1), e1000637.
- Vasalou, C., Herzog, E., Henson, M., 2009. Small-world network models of intercellular coupling predict enhanced synchronization in the suprachiasmatic nucleus. *J. Biol. Rhythms* 24 (3), 243.
- Winfree, A.T., 1967. Biological rhythms and the behavior of populations of coupled oscillators. *J. Theor. Biol.* 16, 15–42.
- Winfree, A.T., 2001. *The Geometry of Biological Time*, 2nd ed. Springer, New York.
- Yamaguchi, S., Isejima, H., Matsuo, T., Okura, R., Yagita, K., Kobayashi, M., Okamura, H., 2003. Synchronization of cellular clocks in the suprachiasmatic nucleus. *Science* 302, 1408–1412.